Climatic Change (2024) 177:33
https://doi.org/10.1007/s10584-024-03688-4

A warm-season drought reconstruction in central-northern Pakistan inferred from tree rings since 1670 CE and its possible climatic mechanism

Adam Khan[1] · Feng Chen[2] · Heli Zhang[2] · Sidra Saleem[3] · Hamada E. Ali[4] · Weipeng Yue[2] · Martín Hadad[5,6]

Received: 5 June 2023 / Accepted: 25 January 2024 / Published online: 15 February 2024

Abstract
Understanding past warm-season drought variability and its underlying climatic mechanisms is crucial for effective drought management and climate adaptation strategies. In this study, we develop a regional chronology (RC) spanning from 1620 to 2017 CE by utilizing dendrochronological techniques and tree-ring data from two stands of *Abies pindrow*. The RC reveals a significant positive correlation ($p < 0.05$) with self-calibrated Palmer drought severity index (scPDSI) and precipitation and a significant negative correlation with temperature. We use a simple linear regression model between RC and climate data to reconstruct a 348-year-long (1670–2017 CE) warm-season (April-July) drought variability from central-northern Pakistan. The reconstructed scPDSI reveals a 44% variance of the scPDSI during the common calibrated period 1950–2017 CE. Spatial correlation shows a positive field correlation with central-northern Pakistan, extending predominantly to neighboring regions. MTM (multi-taper method) spectral analysis reveals inter-annual cycles (6.8, 3.2, 2.7, 2.5, and 2.3 years) and multi-decadal cycles (11.7, 15.2, 16.2, 17.9, and 128 years). The internal-annual cycles demonstrate a possible linkage between reconstructed scPDSI and El Niño–Southern Oscillation (ENSO). The reconstructed scPDSI agrees well with the moisture-sensitive tree-ring records from northern Pakistan and neighboring regions. Our reconstruction shows a significant correlation with the South Asia Summer Monsoon Index (SASMI), Atlantic Multi-decadal Oscillation (AMO), ENSO, Pacific Decadal Oscillation (PDO), and solar activity, emphasizing that all these factors have some influence on the drought variability in central-northern Pakistan. This study has important implications for disaster management and proactive measures for mitigating the impact of drought on both natural ecosystems and human populations in central-northern Pakistan and associated regions.

Keywords Climate change · Dendroclimatology · *Abies pindrow* · scPDSI · Central-northern Pakistan

Extended author information available on the last page of the article

1 Introduction

Warm-season droughts are recurrent natural phenomena that have drastic implications for water resources, agriculture productivity, and the stability of the natural ecosystem. A comprehensive understanding of long-term drought variability and their underlying climatic mechanism is of paramount essential for formulating effective strategies in water management and climate change adaptation. In recent decades, there has been an alarming increase in both the severity and frequency of extreme drought events, resulting in substantial economic losses on a global scale (Easterling et al. 2000; Huang et al. 2016; van der Schrier et al. 2013). Several studies hypothesized that drought is one of the most devastating climate disasters**,** exerting a profound influence on subsistence systems and water resources, leading to societal failures (Gaire et al. 2019; Pederson et al. 2014). Hence, to address the impact of drought on water resources more informedly, long-term drought variability and the potential climatic mechanism that instigates these events become a significant concern (Gaire et al. 2019; IPCC 2007).

The South Asian summer monsoon (SASM) is an integral component of the global climate system (Cook et al. 2010). This phenomenon serves as a dynamic and crucial source of moisture, significantly influencing the Indian subcontinent and the adjacent mountainous regions, including central-northern Pakistan (Betzler et al. 2016; Webster et al. 1998). The SAMS exhibits distinct phases; its active phase is characterized by intense precipitation, resulting in heavy snowfall and floods. In contracts, the break phase is marked by drought, thereby leading to water scarcity issues. The linkage between the atmospheric patterns and the SAMS, particularly the impact of the Atlantic Multi-decadal Oscillation (AMO), El Niño-Southern Oscillation (ENSO), Pacific Decadal Oscillation (PDO), and solar activity, highlights the relationship between global and regional climate drivers (Ahmad et al. 2020; Kumar et al. 2006; Malik et al. 2017; Sinha et al. 2011, 2007; Webster et al. 1998). Hence, understanding of these linkages is essential for predicting extreme weather events and their socioeconomic implication.

Central-northern Pakistan is located between the majestic peaks of the Himalayan and Hindu Kush in the north and spread over the Indus River basin and Karakoram to the south. The region supports the world's largest irrigation network, sustaining millions of livelihoods. Drought reconstruction in central-northern Pakistan using natural proxies such as tree-ring is essential for understanding historical climate variability and its impact on the region. In recent decades, tree-ring-based reconstruction studies have been undertaken in northern Pakistan. For example, some previous studies unlock our understanding of the historical streamflow of the River Indus (Chen et al. 2021; Cook et al. 2013; Rao et al. 2018). The precipitation reconstruction, based on tree-ring width and oxygen isotope chronologies, provides a comprehensive understanding of historical precipitation patterns (Khan et al. 2019; Treydte et al. 2006). However, SASM relieves drier conditions (Wang et al. 2021), while the westerlies bring drier and cooler conditions during winter in northern Pakistan (Treydte et al. 2006). Therefore, knowledge of long-term drought variability in the context of SASM and westerlies is crucial.

Some warm-season temperature reconstruction studies have been carried out in northern Pakistan (Asad et al. 2016; Khan et al. 2021; Zafar et al. 2015). In addition, Ahmad et al. (2020) carried out PDSI reconstruction based on tree-ring *Cedrus deodara* from the Chitral region of Pakistan. However, the study provided valuable information on past drought variability and their teleconnection with AMO, Monsoon Asia Drought Atlas (Cook et al. 2010), and ENSO. Indeed, it is essential to highlight that their study does not

address the impact of the SASM and solar activity on regional drought patterns. These factors are the key drivers of climate fluctuation in the region and need special attention. In addition, regional to large-scale comparisons are vital to obtain broader implications of reconstructed scPDSI. Therefore, in the current study, we sought to answer how *Abies pindrow* responds to scPDSI. We hypothesized that warm-season (April-July) scPDSI could significantly influence the radial growth of *Abies pindrow* and could be a reliable proxy for the reconstruction of the history of scPDSI. To evaluate our hypothesis, we developed the following objectives: (1) to build a new tree-ring chronology from the understudy region of central-northern Pakistan, (2) to evaluate the relationship between radial growth of *Abies pindrow* and scPDSI, (3) to reconstruct the long-term scPDSI variability from central-northern Pakistan, and (4) to demonstrate the possible climate mechanism which significantly affects the regional scPDSI.

2 Materials and methods

2.1 Sampling sites and climate

The sampling sites include two stands of *Abies pindrow*, namely Kot (35° 26′ N, 72° 38′ E, 2430–2734 m a.s.l) and Tuti (35° 36′ N, 72° 59′ E, 2650–2850 m a.s.l) from the Kandia Valley, central-northern Pakistan (Fig. 1 and Table 1). Generally, the lower altitude zone of this region is characterized as drier or arid, whereas the higher altitude zone is moist or humid (Mayer et al. 2010; Winiger et al. 2005). For example, the lower altitude zone (1454 m) of this region received less than the total average precipitation of 137 mm, while more than 720 mm of average precipitation occurred in the high altitude zone (4120 m) (Mayer et al. 2010; Treydte et al. 2006). The monthly climate data of Gilgit station (Fig. 1c) for the period 1955–2017 CE indicate that high precipitation occurred in April (22.7 mm) and May (26.3 mm), and the lowest precipitation was recorded in January (4.8 mm) and December (6.9 mm). The mean monthly maximum temperature (36.1 °C) was observed in July, whereas the mean monthly minimum temperature (− 2.6 °C) was recorded in January.

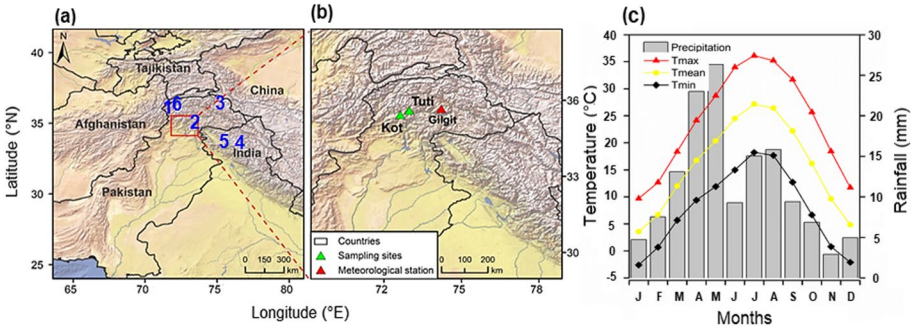

Fig. 1 **a** Map of Pakistan and its neighboring countries, **b** tree-ring sampling sites (Kot and Tuti) for *Abies pindrow* in the Kandia valley of central-northern Pakistan denoted by green triangles, and meteorological station in the Gilgit region marked by red triangles. **c** Climograph of meteorological station near our study area, for the period 1955–2017 CE. In the left map (**a**), blue numbers 1, 2, 3, 4, 5, and 6 correspond to the study sites of Ahmad et al. (2020), Khan et al. (2019), Treydte et al. (2006), Singh et al. (2022), Yadav et al. (2017), and Cook et al. (2010), respectively

Table 1 Sampling sites informations and statistical features of standardized tree-ring width chronologies from the Kandia Valley of central-northern Pakistan

Statistical items	Kot chronology	Tuti chronology	RC
Latitude (N)	35° 26′ N	35° 36′ N	-
Longitude (E)	72° 38′ E	72° 59′ E	-
Altitude ranges (m)	2430–2738	2650–2850	2430–2850
Aspect	NW	NW	NW
Core samples/trees	24/16	43/30	67/46
Chronology span	1620–2017	1616–2017	1616–2017
Series-inter correlation	0.610	0.566	0.598
Rbar between trees	0.274	0.323	0.309
Standard deviation (SD)	0.348	0.353	0.350
Mean sensitivity (MS)	0.213	0.210	0.211
Signal-to-noise ratio (SNR)	7.593	15.731	15.658
Variance in first Eigenvector (%)	74.3	73.1	73.8
First year where EPS > 0.85 (no of trees)	1710 (3)	1670 (3)	1670 (4)
Missing rings (%)	2 rings (0.03%)	45 rings (0.39%)	47 rings (0.26%)

In northern Pakistan, there are two observation stations, namely Gilgit (35° 55′ N, 74° 20′ E, 1454 m a.s.l) and Astore (35° 24′ N, 74° 54′ E, 2000 m a.s.l.). These observation stations are relatively distant (Gilgit = 256 km; Astore = 233 km) from our study area. The observation records from these stations contain some missing data, which we addressed by averaging data from the prior year and subsequent year. No fixed distance for the observation station is universally applicable. However, the observation station located in proximity (10–20 km) to the sampling site is mostly preferred. This approach is more likely to present the microclimate condition experienced by taxa. Due to the considerable distance between our sampled sites and observation stations, we obtained a climate dataset from CRU TS4.07 (averaged over 33.5°–34.5°N, 72.0–73.0°E) via KNMI climate explorer (van der Schrier et al. 2013). The climate data (temperature and precipitation) from CRU TS4.07 and the Gilgit observation station suggested a significant relationship ($p > 0.01$), whereas no meaningful relationship was observed between CRU TS4.07 and the Astore observation station. The Z-scores analysis of climate data from Gilgit and CRU TS4.07 demonstrated an increase in temperature and rainfall in recent decades, while the data from the Astore observation station showed a decline in rainfall (Fig. 2). A significant decline in rainfall was observed from 1955 to 1972 CE.

2.2 Tree-ring data

Abies pindrow (Royle), also known as west Himalayan fir, is widely distributed from India to central Nepal and Afghanistan to Pakistan. It generally grows from dry to moist temperate regions ranging from 2000 to 3300 m a.s.l (Ahmed 1989; Xiang et al. 2013). Two core samples were extracted from each tree; however, for a few young trees confined on a very steep slope, we obtained only one core. A total of 82 core samples were extracted from 46 living via using the 5-mm-diameter Haglöf Sweden increment borer.

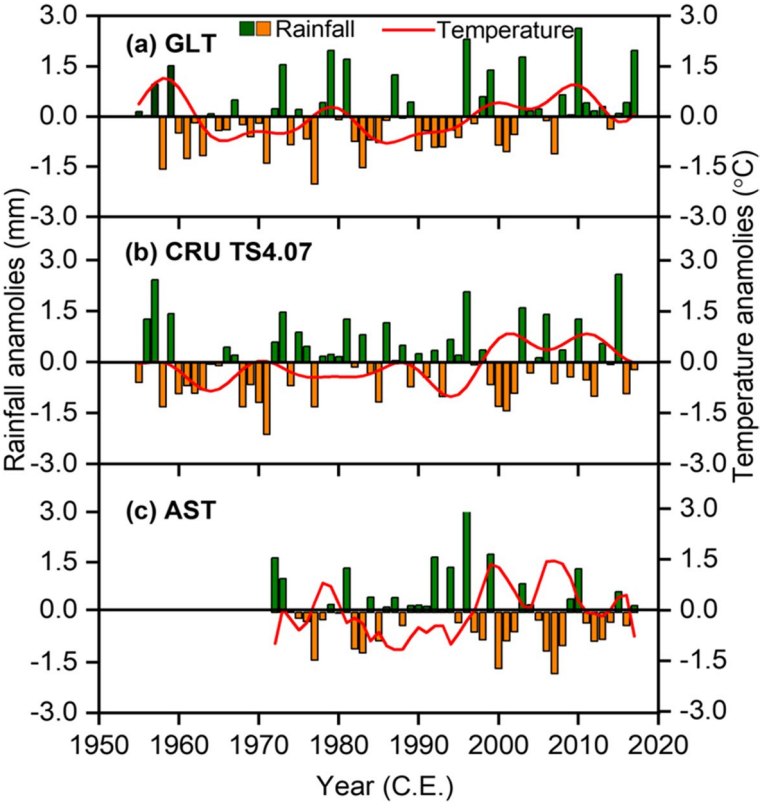

Fig. 2 Graphical comparison (z-scores) between rainfall and temperature of (**a**) Gilgit (GLT), (**b**) CRU TS4.07, and (**c**) Astore (AST) stations. The green and orange bars represent moist and drought conditions, respectively, and the bold line indicates temperature fluctuation over time

The collected samples were air-dried at room temperature, mounted with glue, and polished with progressive sandpaper (320 grit) (Fritts 1976; Speer 2010). After polishing the core samples, clear and distinct rings appeared. The width of the tree ring was measured with a high level of precision (i.e., 0.001 mm accuracy) using the LINTAB tree-ring measuring system. The cross-dating of collected core samples was performed through TSAP software. Of the 82 core samples, 67 were successfully cross-dated (Table 1). A few samples exhibiting anomalous growth, missing rings, and false rings were rejected and not included in our analysis. The quality and coherence of cross-dating were checked with COFECHA software (Holmes 1983) The standard chronology of each site was developed by using ARSTAN software (Cook et al. 1990). The interstands correlation of obtained chronologies revealed a high and significant relationship ($r = 0.893$, $n = 399$, $p < 0.01$). Consequently, all series of tree-ring growth were combined to construct a regional chronology (RC). In order to remove non-climatic trends, the negative exponential curve was applied. To assess the mean correlation and strength of the common signal between all tree-ring series, expressed population signal (EPS)

and Rbar (inter-series correlation) were calculated with ARSTAN software (Cook and Kairiukstis 1990; Wigley et al. 1984).

2.3 Reconstruction methodology

The Pearson's correlation coefficient analysis between RC and climate dataset was conducted for the common period 1950–2017 CE. A strong correlation was observed between RC and the CRU TS4.07 climate dataset. Therefore, in this study, we utilized the CRU TS4.07 climate dataset. Correlation coefficients were calculated from the prior year, October, to the current year, September, via DENDROCLIM2002 software (Biondi and Waikul 2004). For reconstruction, we used a simple linear regression model, the RC index as a predictor, and the mean scPDSI of April-July was used as a predictant. The reliability of our reconstruction was determined with split calibration-verification tests through the validation method. The statistical analysis includes R^2 (coefficient of multiple determination), RE (reduction of error), CE (coefficient of efficiency), and sign test (Cook and Kairiukstis 1990). The positive value of RE and CE showed the stability and effectiveness of our reconstruction. The Durbin-Watson statics, which reflect the autocorrelation in the residual, showed the reliability of our reconstruction. Based on scPDSI values, the reconstructed scPDSI were characterized as incipient, mild/slight, moderate, severe, and extreme drought (van der Schrier et al. 2013). The "−0.5 to 0.5" value of scPDSI is normal, and the negative value of scPDSI indicates drought. For example, the scPDSI value of −0.5 to −1.0 is incipient drought, −1 to −2 is mild drought, −2 to −3 is moderate drought, −3 to −4 is severe drought, and < −4 indicates extreme drought. The positive values of scPDSI indicate wet periods (van der Schrier et al. 2013). In order to identify the spatial representation of our reconstructed scPDSI with CRU TS4.07 scPDSI and sea surface temperature, spatial correlations were determined for the common period 1955–2017 CE using KNMI climate explorer (https://climexp.knmi.nl). The periodicities cycles in our reconstruction were estimated with multi-taper method spectral analysis (MTM) (Mann and Lees 1996).

3 Results

3.1 Tree-ring chronology and its response to climatic variables

The length of the tree-ring chronology from the Kot site was 1616–2017 CE, while for the Tuti site, it was 1620–2017 CE (Supplementary Fig. S1). To ensure the reliability of RC, the developed RC was truncated prior to 1670 via EPS threshold limit (EPS > 0.85) (Fig. 3). The RC had a high series-inter correlation (0.566–0.610). The variance in the first eigenvector (73.1–74.3%) and standard deviation (0.210–0.213) demonstrated that the ring widths of *Abies pindrow* are responding to common climate factors (Table 1). Furthermore, the RC reveals extremely narrow ring in specific years, including 1677–1678, 1697–1699, 1705, 1726–1727, 1802, 1815, 1820, 1841, 1853, 1855, 1872, 1892, 1947, 1953, and 2001–2002.

The RC exhibits a significant positive correlation ($p < 0.05$) with precipitation from the prior year, October, and March–May of the current year (Fig. 4a). In contrast, the RC demonstrated a significant negative correlation with minimum temperature (T_{min}) during the prior year, October–November, and the current year, April–May. Furthermore, the RC showed a significant negative relationship with the maximum temperature (T_{max}) of

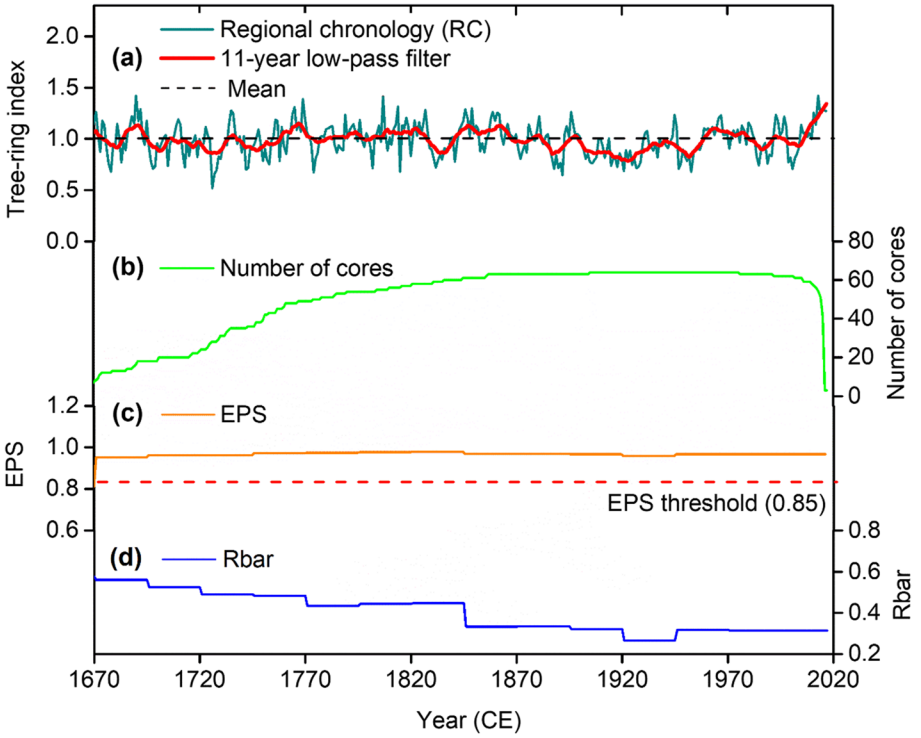

Fig. 3 **a** RC plot of *Abies pindrow* from the Kandia valley of central-northern Pakistan, (**b**) sample depth, (**c**) running expressed population signal (EPS), and, (**d**) Rbar (mean correlation between ring-width series) statistics

the prior year, December, and the current year, March–May (Fig. 4b). A notably strong and statistically significant correlation was found between RC and scPDSI. The RC revealed a stronger correlation with the mean monthly scPDSI ($r=0.666$, $p<0.001$) of warm season (April–July) than precipitation ($r=0.311$, $p<0.05$), minimum temperature ($r=-0.338$, $p<0.05$), and maximum temperature ($r=-0.306$, $p<0.05$). This indicates that scPDSI of warm season is the fundamental factor influencing the radial growth of *Abies pindrow*.

3.2 scPDSI reconstruction

Based on the growth-climate analysis, we selected the mean scPDSI of April–July for the reconstruction via linear regression model. The transfer function was

$$\mathrm{scPDSI}_{4-7} = -9.12 + 9.42\mathrm{RC} \quad (1)$$

where $\mathrm{scPDSI}_{4\text{-}7}$ is the April–July self-calibrated Palmer drought severity index (scPDSI), and RC is the standard regional chronology of *Abies pindrow*. The reconstruction model accounts for 44% variance for the actual scPDSI during the common period 1955–2017 CE ($n=67$, $F=52.549$, $p<0.001$). The reconstructed scPDSI fit well on the actual scPDSI curve except for a few extraordinarily high values (Fig. 5a). Durbin-Watson value (Durbin

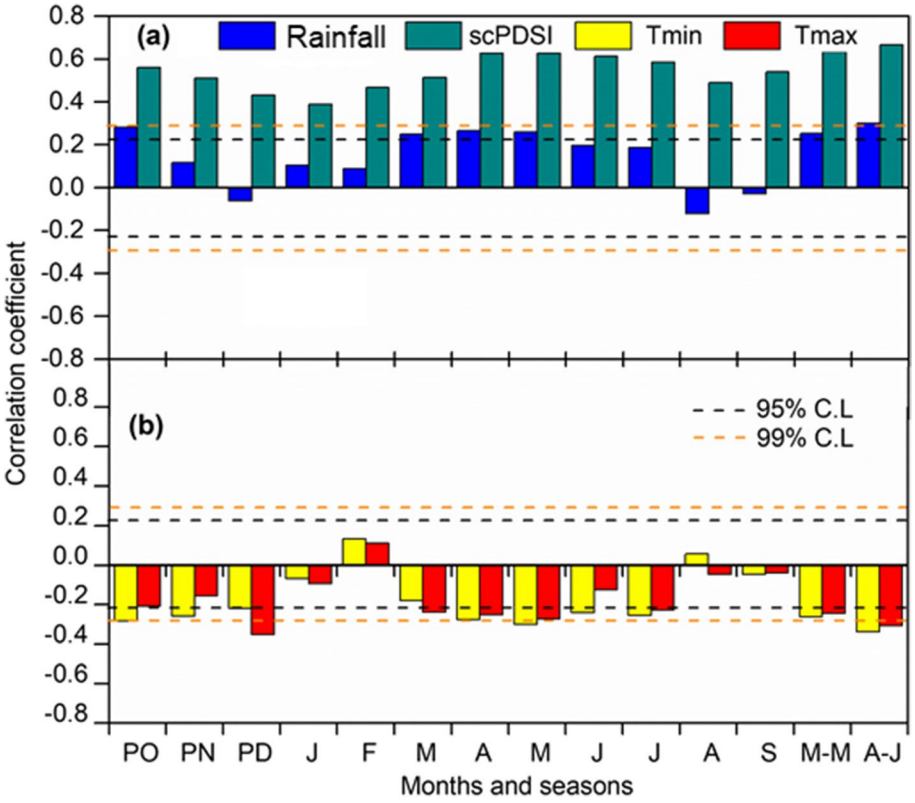

Fig. 4 **a** The correlation coefficient between the RC and total monthly precipitation and mean monthly scPDSI and (**b**) correlation coefficients between the RC and mean monthly minimum temperature (Tmin) and maximum temperature (Tmax). The correlation coefficients were computed from the prior year October to the current year September over the common period 1950–2017 CE. The black and orange horizontal dashed lines reveal significance level at the 95% and 99% confidence limits (C.L), respectively. The M-M represents the correlation coefficient for the months of March–May, whereas the A–J shows the correlation coefficient for the months of April–July

and Watson 1950), which revealed the autocorrelation of the reconstruction, was 2.154. The statistical analysis demonstrated that the actual and reconstructed scPDSI are synchronous at low-frequency variations. The positive value of the RE and CE further confirmed the stability and validity of our climatic reconstruction model (Table 2). The long-term reconstructed scPDSI showed consistency with the actual scPDSI. Therefore, this study is valuable to understand the drought variability over several hundred years in central-northern Pakistan.

3.3 Characteristics of reconstructed scPDSI sequence

The long-term mean of the reconstructed scPDSI was 0.24, with a standard deviation (σ) of 1.50, indicating low-frequency drought variability over the past 348 years (Fig. 5b). The periods 1729–1730, 1752–1753, 1775–1776, 1829–1830, 1905–1908, 1950–1952, 1990–1991, and 1999–2000 showed mild drought. Besides, 1674–1675,

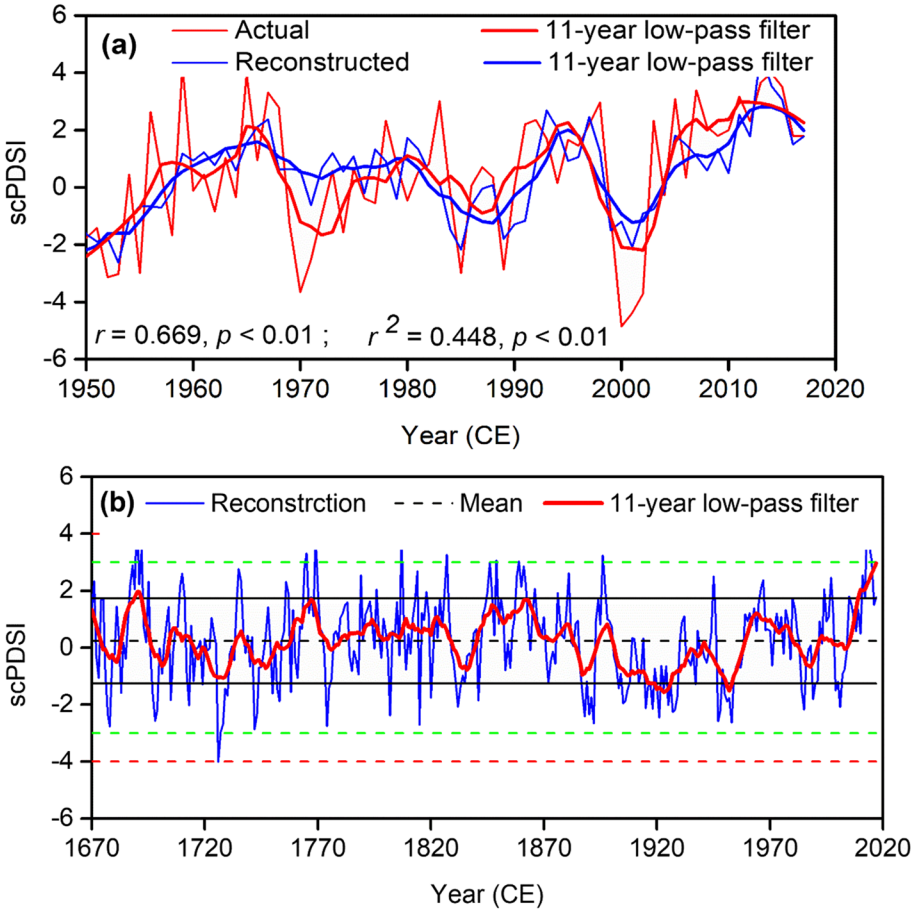

Fig. 5 **a** Actual (red) and reconstructed (blue) warm-season (April–July) self-calibrated Palmer drought severity index (scPDSI) over the common calibration period 1950–2017 CE. **b** Long-term reconstructed warm-season scPDSI from the Kandia valley, central-northern Pakistan. Both the actual and reconstructed scPDSI were smoothed with 11-year low-pass filter. The central black horizontal dotted line represents the mean of long-term scPDSI reconstruction (0.24). The black solid lines show the mean value of $\pm 1\sigma$ (1.50). The lime-dotted lines represent the threshold limit for severe drought or wet condition, and the red-dotted lines reveal threshold lines for extreme drought or wetter condition, followed by standard scPDSI categorization (van der Schrier et al. 2013)

1766–1768, 1780–1783, 1791–1793, 1867–1869, 1878–1879, 1882–1885, 1909–1910, and 1968–1970 revealed mild wet conditions. Moderate drought periods were observed in 1677–1678, 1698–1699, 1727–1728, 1742–1743, 1927–1928, and 1947–1948, while moderate wet periods occurred in 1687–1689, 1709–1710, 1735–1736, 1860–1862, and 1966–1967. Furthermore, extreme drought in central-northern Pakistan occurred in 1705, 1726, and 1815, while the wettest conditions were observed in 1724, 1807, and 2013. Throughout the reconstruction, 1890–1940 was the long-lasting drought period in central-northern Pakistan.

Table 2 Statistical characteristics of (a) leave-one-out cross-validation and (b) split calibration–validation methods for the scPDSI reconstruction from the Kandia Valley of central-northern Pakistan

	Calibration (1950–1983)	Validation (1984–2017)	Calibration (1984–2017)	Validation (1950–1983)	Full calibration (1950–2015)
r	0.576	0.757	0.757	0.576	0.666
R^2	0.331	0.573	0.573	0.331	0.443
R^2_{adj}		0.560		0.311	0.435
DW		1.854		2.127	2.154
F value		42.995**		15.868*	52.549*
RE		0.560		0.257	
CE		0.400		0.253	
Sign test		$28^+/6^-$ **		$17^+/17^-$ *	
First-order sign test		$20^+/13^-$ *		$20^+/13^-$ *	

R^2_{adj}, R^2 adjusted; *DW*, Durbin-Watson; *RE*, reduction of error; *CE*, coefficient of efficiency

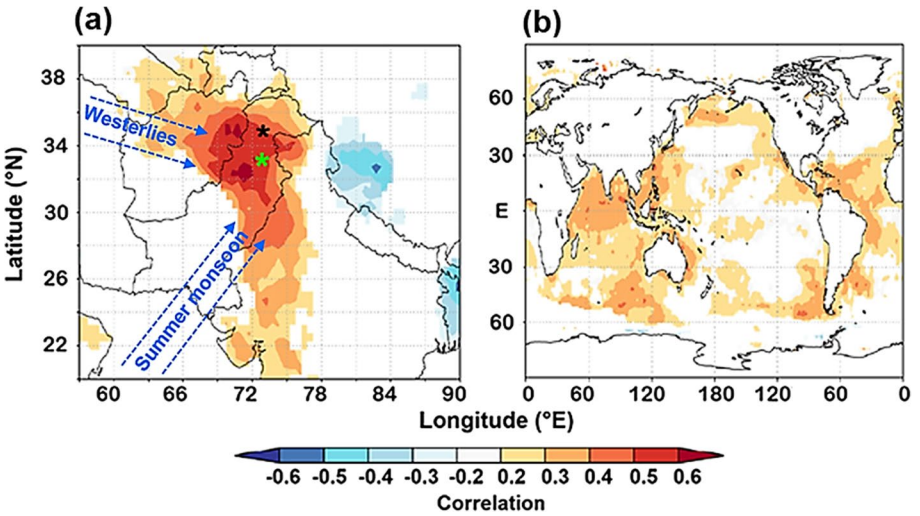

Fig. 6 **a** Spatial correlations ($p < 0.05$) between reconstructed and regional gridded (CRU TS 4.01) warm-season scPDSI during the common period 1901–2017 CE and (**b**) reconstructed warm-season scPDSI with sea surface temperature (HadISST1) during the common period 1870–2017 CE. The black and lime stars in the left map demonstrate tree-ring sampling site and the capital (Islamabad), respectively

The spatial correlation between the reconstructed and CRU TS4.07 gridded scPDSI from April to July demonstrated a positive field correlation, extending predominantly north–south (Fig. 6a). Meanwhile, the reconstructed scPDSI revealed a negative field correlation with certain regions in Bhutan and India. The possible reason could be the influence of local topography, which leads to the effects of rain shadows and variation in regional rainfall. In addition, short-term climate anomalies and monsoonal patterns have drastic effects on regional moisture variability, resulting a negative association. However, to identify the precise causes of this negative relation, a detailed climatological

investigation is needed. The spatial relationship between reconstructed scPDSI and sea surface temperature (SST) can contribute to the influence of SST patterns on regional climate.

Furthermore, a spatial correlation analysis was conducted between the reconstructed scPDSI and SST data (HadISST1) for the period April–July (Fig. 6b). The results revealed a significant positive correlation between our reconstructed scPDSI and the northern Indian Ocean, as well as the western tropical Pacific Ocean. This implies that these regions are important sources of water vapor for central-northern Pakistan. Changes in SST have the ultimate impact on atmospheric circulation, leading to a change in rainfall pattern. For instance, warmer SST might improve moisture transport and result in considerable rainfall in a specific region. This relationship highlighted the connection between distinct ocean and terrestrial climate systems and emphasized the significance of large-scale oceanic factors in shaping regional to large-scale climatic conditions.

The MTM spectral analysis (Mann and Lees 1996) revealed inter-annual cycles (6.8, 3.2, 2.7, 2.5, and 2.3 years) and multi-decadal cycles (11.7, 15.2, 16.2, 17.9, and 128 years) in the reconstructed scPDSI from the Kandia Valley in central-northern Pakistan (Fig. 7).

4 Discussion

4.1 Regional chronology (RC) and its response to climate variables

The regional chronology (RC), developed from tree-ring data of two stands of *Abies pindrow*, spans from 1620 to 2017 CE. The statistical parameters of the RC, including Rbar between tress, mean sensitivity (MS), standard deviation (SD), and signal-to-noise ratio (SNR), underscored the high dendroclimatic potential of *Abies pindrow* (Fritts 1976). The characteristics of the RC fall within the range observed in previous dendroclimatic studies of the same species and other species in Pakistan (Ahmad et al. 2020; Ahmed 1989; Chen et al. 2021; Khan et al. 2021; Zafar et al. 2015). The extremely narrow rings recorded in the RC were attributed to drought conditions (Fritts 1976; Shi et al. 2014), as detected during moderate and extremely drought epochs in our reconstruction. The narrow rings recorded

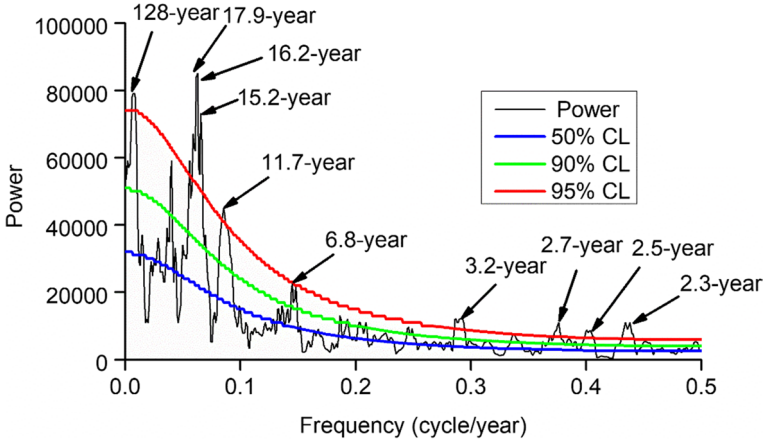

Fig. 7 MTM power spectral analysis for the reconstructed warm-season scPDSI from the Kandia Valley, central-northern Pakistan

in our study may be linked with regional to large-scale climate variability. For instance, the extremely narrow ring (2001) was observed by previous studies in northern Pakistan (Ahmad et al. 2020; Esper et al. 2003; Khan et al. 2013; Zafar et al. 2010). Furthermore, the extremely narrow ring recorded in the year 1705 was consistent with the scPDSI study of the trans-Himalayan region of central Himalaya (Gaire et al. 2019). Similarly, the narrow ring (1947) was recorded in the western Tian Shan Mountain of Kyrgyzstan (Zhang et al. 2017). The resemblance of these narrow rings indicated the influence of large-scale climate variability over central-northern Pakistan.

The radial growth of *Abies pindrow* showed a significant positive correlation with precipitation from the prior October and March–May of the current year. Meanwhile, the radial growth of *Abies pindrow* revealed a significant positive correlation with scPDSI from the prior year, October, to the current year, September. In contrast, there is a significant negative correlation with temperature from prior October–December and March–July of the current year. Notably, the radial growth of *Abies pindrow* showed a substantial positive correlation with scPDSI and precipitation and a negative correlation with temperature during April–July, indicating that scPDSI is the essential climate factor. Similar results have been observed in the studies conducted in Pakistan and neighboring countries (Ahmad et al. 2020; Chen et al. 2016; Gaire et al. 2019; Khan et al. 2019; Singh et al. 2017). Studies are evident that in the high-altitude region, the radial growth of tree initiates in spring and stops at the end of summer (Ahmed et al. 2011; Gutiérrez et al. 2011). However, it is obvious that at the timberline, the radial growth of the tree is sensitive to temperature (Asad et al. 2016), while below the timberline, it is mostly influenced by scPDSI and precipitation, especially during the growing season (Bhandari et al. 2020; Khan et al. 2019). Studies showed that below the timberline in arid-semiarid regions, temperature plays an opposing role in the radial growth of trees as it serves as a key factor in intensifying drought and increasing evapotranspiration (Fang et al. 2012; Ram 2012; Shi et al. 2016). Hence, there is an apparent negative correlation with radial growth. However, below the timberline, the scPDSI reflects the balance between rainfall, soil moisture, and evapotranspiration and exhibits a positive correlation with radial growth of tree. In addition, it is noteworthy that during April–July, trees allocate a significant portion of their energy to radial growth, which necessitates enough water for photosynthesis and the transport of nutrition via vascular system. However, when scPDSI indicates limited moisture content, it reduces the radial growth of tree due to insufficient moisture content and delay photosynthesis, resulting narrow rings formation.

4.2 Drought variability for the Kandia Valley central-northern Pakistan since 1670 CE

The tree-ring reconstructed April–July scPDSI is linked to a scPDSI field situated approximately north of the 30–36° latitude, characterized by a significant southeast-northwest extension. The reconstruction revealed a strong association with central-northern Pakistan. In accordance with the standard classification of drought, our scPDSI reconstruction demonstrated eight mild drought periods and six moderate drought periods (van der Schrier et al. 2013). The notable mild drought period from 1905 to 1908 CE was coherent with a dry period documented in the tree-ring-based drought reconstruction of Tien Shan Mountain, Kazakhstan (Chen et al. 2016). In addition, the drought period spanning from 1920 to 1930 CE was reported from northern China (Liu et al. 2009; Yang et al. 2011; Zhang et al. 2011) and northeastern Mongolia (Pederson et al. 2001). This drought affected a

wide area of China, resulting in economic damage and marvelous loss of life (Liang et al. 2006; Shi et al. 2016). Our study shows that the evidence of the drought period occurred in 1920–1930 CE. However, no record of high-intensified drought and economic losses is available from central-northern Pakistan. The most prominent feature observed in our reconstructed scPDSI is the increase of high-magnitude droughts in the early eighteenth century, which persisted to the mid-nineteenth century with some dominant wet phases. Nevertheless, a prolonged increasing drought trend was observed in the late nineteenth century and early twentieth century. The same drought trend has been observed in tree-ring-based drought studies in other countries (Gaire et al. 2019; Sano et al. 2012; Yadav et al. 2017). The drought trend observed in the late eighteenth and early nineteenth centuries is similar to the study of northern Pakistan (Treydte et al. 2006). Persistent evidence of moderate drought (1920–1930 CE) in the early twentieth century was observed in the tree-ring-based drought study of the Chitral region (Ahmad et al. 2020). However, it was not as prominent as in this study. The possible reason for this discrepancy may be differences in the standardized categorization of drought events. The recorded wettest years, such as 1724, 1807, and 2013, coincide with other reconstructions of central Asia, Nepal, and the Chitral region of northern Pakistan (Ahmad et al. 2020; Chen et al. 2019). According to Treydte et al. (2006), twentieth-century warming could increase the moisture-holding capacity of the atmosphere. A similar increasing moisture trend was observed in our reconstruction (Fig. 5), as well as in the anomalies of meteorological station data (Fig. 2).

4.3 Periodicities in the drought reconstruction of central-northern Pakistan

The detected annual periodicity cycles, ranging from 2.3 to 2.7, 3.2, and 6.8 years, indicated potential links to quasi-biennial oscillations and El Niño–Southern Oscillation (ENSO), which are the key drivers of climate variability (Allan et al. 1996; Burgers et al. 2005). The climate of central-northern Pakistan is mutually influenced by the SASM and westerly patterns. Therefore, the observation of high-frequency periodicity cycles in our study demonstrated that drought variability in our study area may be responsive to large-scale ocean–atmosphere–land circulations. The 11.7-year cycle showed a resemblance with the 11-year solar activity cycle, hinting at a potential linkage between local drought changes and solar activity. In addition, the centennial–scale cycle (128 years) recorded in our reconstruction resembles similar findings in the surrounding Tibetan Plateau, emphasizing the complex and interrelated nature of climate patterns (Fang et al. 2010; Peng and Liu 2013).

4.4 Regional to large-scale comparison

The drought formation may be potentially influenced by common factors at the regional or large scale (Borgaonkar et al. 2010; Cai et al. 2015; Gaire et al. 2019; Peng and Liu 2013). Therefore, in order to achieve a more holistic prospect of drought variability, it is essential to consider both regional and large-scale perspectives. On the regional scale, our reconstructed April–July scPDSI showed a significant positive correlation ($r = 0.307$, $p < 0.01$) with the reconstructed March–August scPDSI from the Chitral region (Ahmad et al. 2020) (Table 3). However, it is essential to note that some of the dry phases in our reconstructed scPDSI do not align with the study of Chitral (Ahmad et al. 2020) (Fig. 8a). For example, the dry phases, including 1670–1690, 1710–1730, 1830–1850, and 1920–1930 CE, identified in our study and previous studies from Pakistan and neighboring regions (Cook et al.

Table 3 Correlation between our reconstructed scPDSI and prior studies conducted in Pakistan and the neighboring regions

	Ahmad et al. 2020	Khan et al. 2019	Treydte et al. 2006	Singh et al. 2022	Cook et al. 2010	Yadav et al. 2017
Z-scores (raw)	0.307**	0.254**	−0.150*	0.334**	0.236**	0.995**
11-year low-pass filter	0.279**	0.180**	−0.076	0.223*	0.157**	0.998**
n	347	329	336	348	348	348

* Significant at 0.05, ** Significant at 0.01

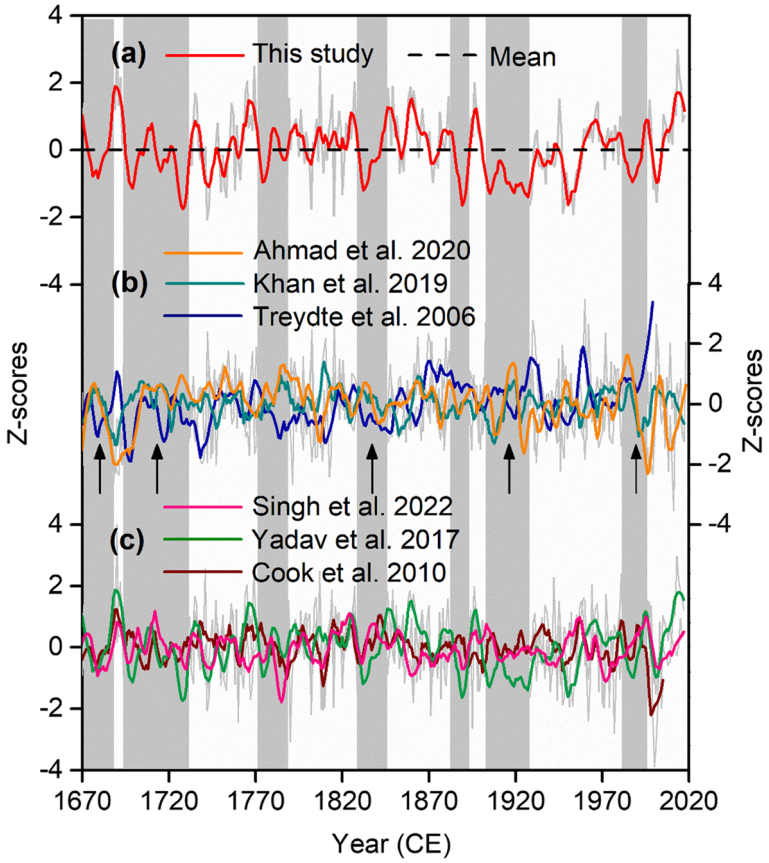

Fig. 8 Graphical comparison between the central-northern Pakistan scPDSI reconstruction (this study), **a** tree-ring-based precipitation and drought studies from Pakistan, and (**b**) drought reconstruction from nearby regions

2010; Khan et al. 2019; Singh et al. 2022; Treydte et al. 2006; Yadav et al. 2017), are not actually dry in the reconstruction of Chitral (Ahmad et al. 2020). Moreover, our reconstruction revealed a significant positive correlation ($r = 0.254$, $p < 0.01$) with the June–May precipitation of Khan et al. (2019). However, with the exception of a few phases, most of the dry phases are aligned with our reconstruction. A weak and negative correlation ($r = -0.150$, $p < 0.01$) was found between our reconstructed scPDSI and October–September reconstructed precipitation from the Karakoram region (Treydte et al. 2006). This negative correlation may be attributed to the utilization of different approaches for climate reconstruction and differences in local climate. For instance, the reconstructed precipitation of Karakoram (Treydte et al. 2006) was based on annually resolved oxygen isotope, while the scPDSI reconstruction of our study is based on annual growth data. Furthermore, variation in regional and topographic features leads to weak correlation. According to Shah et al. (2010), the pre-monsoon season during April–July is a transitional phase from the winter circulation to monsoon circulation in the region. During this phase, westerly waves move northward, and the frequency of western disturbance decreases in comparison to the winter peak months. The weak correlation between our reconstruction and Treydte et al.

(2006) could be attributed to this transitional phenomenon. In addition, it is important to note that our sampling site is located about 650 m and 750 m below the elevation range of the sites studied by Ahmad et al. (2020) and Treydte et al. (2006), respectively. This means that our sampling site experienced high evapotranspiration compared to the sites they studied.

The comparative analysis of the reconstructed scPDSI from central-northern Pakistan in this study with the northwest Himalaya of India, the northwest Himalaya and Karakoram region of India, and the Monsoon Asia Drought Atlas showed a high degree of consistency at both inter-annual and inter-decadal scales (Fig. 8b). Most of the drought phases identified in our reconstruction align with the findings of these studies. Notably, our reconstructed scPDSI exhibited a strong positive relationship with the June–May drought (Singh et al. 2022), the standardized precipitation index (SPI) of May (SP18-May) (Yadav et al. 2017), and the June–August drought (MADA) (Cook et al. 2010) highlighting the robustness of our reconstruction and elucidating the spatial and regional patterns of hydroclimatic variability (Table 3). After applying an 11-year low-pass filter, the correlation between our reconstruction and the one presented by Yadav et al. (2017) has increased, whereas the correlations with other moisture-sensitive tree-ring records decreased.

4.5 Possible climatic mechanism

Climatic mechanisms play a significant role in shaping the intensity and duration of drought events. Identifying these potential climatic drivers is crucial. To evaluate these potential drivers and their influence on drought variability, a correlation analysis was carried out between our reconstructed scPDSI and various indices, including SASMI, AMO, PDO, NINO, and NAO.

Our reconstruction reveals a significant positive correlation ($r = 0.37$, $p < 0.01$) with SASMI (Fig. 9a). The peiods of low SASMI, notably during 1950–1958, 1983–1993, and 1999–2004 CE, were consistent with the dry phases identified in our warm-season scPDSI reconstruction. Similarly, the observed high SASMI from 2005 to the present align with our reconstruction. However, in comparison to SASMI, our reconstruction exhibits a weak linkage with the Indian summer monsoon (ISM). This discrepancy may be attributed to the regional sensitivity of our reconstruction, which aligns more closely with SASMI and appears to be less influenced by the broader dynamics of the ISM (Khan et al. 2019). However, to fully validate and understand this explanation, further research is needed.

Furthermore, our warm-season scPDSI exhibits a significant positive correlation ($r = 0.41$, $p < 0.01$) with AMO (Fig. 9b). On a decadal scale, the drier phases observed in our warm-season scPDSI reconstruction exhibit notable consistency with the negative phases of the AMO, particularly during 1880–1895, 1902–1930, 1946–1950, and 1989–1997 CE. This association implies a potential link between the negative phases of AMO and the occurrence of drier conditions in central-northern Pakistan. A study conducted in the Chitral region of Pakistan indicated a possible linkage between reconstructed drought and SASMI and AMO (Ahmad et al. 2020). However, its essential to note that their analysis was based on low-frequency variability, specifically a 31-year moving average. Additionally, their reconstruction reflects variation aligning with certain phases of AMO and SASMI.

A number of studies highlight the influence of ENSO on regional moisture change, emphasizing temporal variability (Krishna and Rao 2010; Kumar et al. 2007; Sano et al. 2009). Our warm-season scPDSI reconstruction generally aligns with the prominent phases

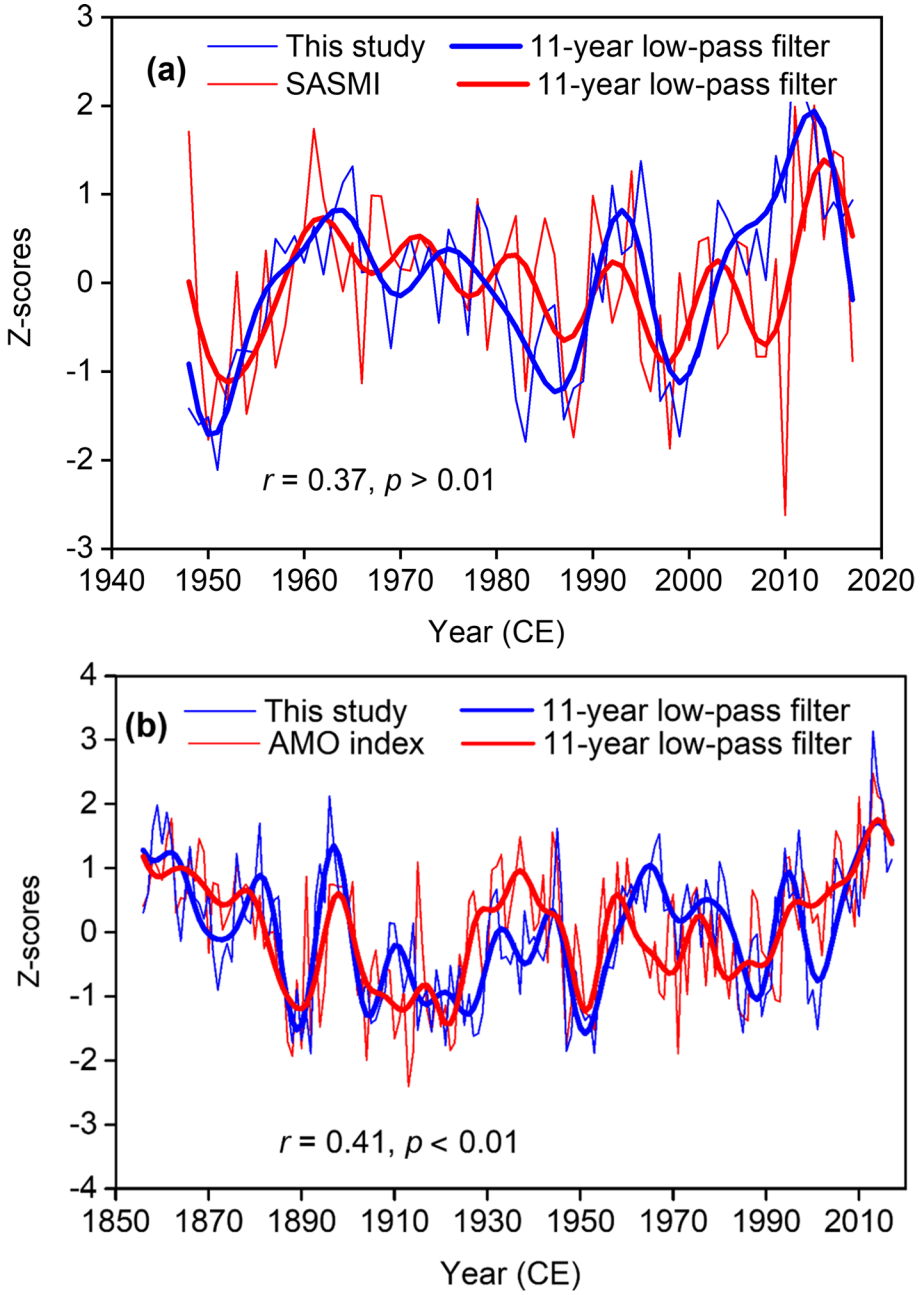

Fig. 9 **a** Comparison (Z-scores) between the reconstructed warm-season scPDSI (this study) with South Asia Summer Monsoon index (SASMI) (Li and Zeng 2002) and (**b**) Atlantic Multi-decadal Oscillation (AMO) (van Oldenborgh et al. 2009). All series were smoothed with 11-year low-pass filter

of ENSO, particularly NINO 3.4 (Supplementary Fig. S2). Studies have shown that ENSO is the potential drivers that has a significant influence on hydrological changes associated with AMO (Chen et al. 2019; Palmer et al. 2015; Shi et al. 2018). According to Shi et al. (2014), drought coincided with the warm phase of ENSO, linked to Indian summer monsoon failure. This implies that the recent increasing moisture trend in central-northern Pakistan is potentially associated with ENSO. Additionally, the robust relationship of our reconstruction with specific months of NINO4, NINO3.4, and NINO3 provides additional confirmation (Table 4).

The Pacific Decadal Oscillation (PDO) is also an important climate driver influencing atmosphere circulation, sea temperature, and rainfall patterns, thereby impacting drought variability in different regions (de Oliveira-Júnior et al. 2018; Schoennagel et al. 2005). Our reconstruction reveals a noteworthy relationship with specific months of the PDO (Table 4), showing a substantial link between PDO and drought variability in central-northern Pakistan. Despite the North Atlantic Oscillation (NAO) not profoundly affecting the climate of the northern hemisphere, including central-northern Pakistan. Our reconstruction still exhibits a significant correlation with the June month of NAO. This correlation might be attributed to similar atmospheric circulation and rainfall patterns between the northern and southern hemispheres.

The solar modulation function and sunspot number are important factors that have a significant influence on climate dynamics (Hong-yan et al. 2015; Muscheler et al. 2007). Historical long-term records of the solar modulation function and sunspot number show considerable variation (Fig. 10a, b), notably characterized by the Maunder minimum (1645–1715 CE), the Dalton minimum (1790–1820 CE), and the Damon minimum (1900–1920 CE) periods. The prolonged drought periods identified in our reconstruction coincide with reduced solar activity, suggesting a potential link between drought and solar variation. Furthermore, the solar modulation function and sunspot number indicate maximum solar activity during 1760–1800 CE and from 1950 to the present. Notably, solar activity during 1760–1800 CE exhibited a higher intensity than that revealed in recent decades. This potentially reflects the intricate natural variability inherent in solar cycles, characterized by their intermittent nature. Our scPDSI reconstruction demonstrates drought condition during the period of stronger solar activity, contrasting with wetter condition in recent decades (Fig. 10c). These insights enhance our understanding of the intricate relationship between

Table 4 Correlation between reconstructed scPDSI (this study) and the climatic drivers

Months	PDO	NINO4	NINO3.4	NINO3	NAO
January	0.400**	0.297*	0.320**	0.272*	−0.099
February	0.076	0.292*	0.192*	0.278**	0.009
March	0.150	0.353**	0.196*	0.052	0.015
April	0.198*	0.336**	0.276**	0.090	0.035
May	0.195*	0.252*	0.243**	0.241*	0.051
June	0.095	0.170	0.196*	0.255**	0.178*
July	0.086	0.154	0.110	0.098	0.073
August	0.013	0.141	0.057	0.070	−0.093
September	0.028	0.109	0.052	0.073	0.039
October	−0.016	0.111	0.065	0.099	−0.072
November	−0.001	0.098	0.081	0.119	−0.048
December	−0.087	0.052	0.076	0.096	0.097

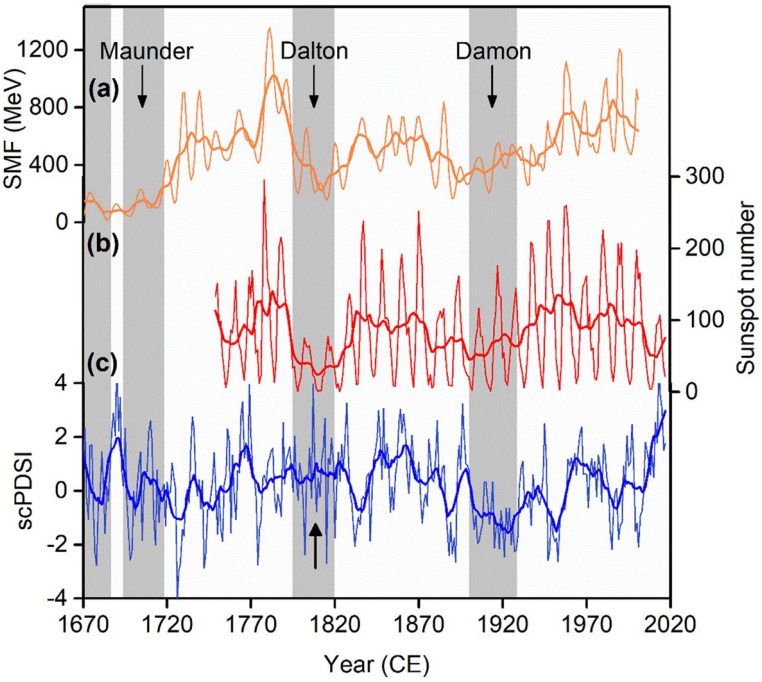

Fig. 10 **a** Graphical comparison between the solar activity and (**b**) sunspot number with (**c**) our scPDSI reconstruction. All series were smoothed with 11-year low-pass filter

variations in the solar cycle and drought variability in central-northern Pakistan, emphasizing the imperative for future in-depth research on these complex connections.

5 Conclusions

We developed a regional chronology (RC) from two stands of *Abies pindrow* in the Kandia Valley, central-northern Pakistan. Growth-climate analysis revealed that warm-season (April–July) scPDSI is the fundamental factor that significantly influences the radial growth of *Abies pindrow*. Using linear regression, we reconstructed a 348-year (1670–2017 CE) long-term warm-season scPDS variability. The reconstructed scPDSI explained a 40% variance in the actual scPDSI during the common period of 1950–2017 CE. Furthermore, the multi-taper method (MTM) spectral analysis identified distinct cycles of inter-annual (6.8, 3.2, 2.7, 2.5, and 2.3 years) and multi-decadal (11.7, 15.2, 16.2, 17.9, and 128 years). The inter-annual cycles revealed possible links between central-northern Pakistan and the El Niño-Southern Oscillation (ENSO), as confirmed by correlation analysis of our scPDSI reconstruction with ENSO and the Pacific Decadal Oscillation (PDO). In addition, our scPDSI reconstruction revealed significant links with the South Asian Summer Monsoon (SASMI), as well as the Atlantic Multidecadal Oscillation (AMO). These findings indicate that SASM and AMO are the key drivers that significantly influencing drought variability in central-northern Pakistan. Furthermore, we also observed that some prolonged drought events are consistent with period of reduced solar activity and sunspot numbers.

These findings enhance our understanding of long-term drought variability and its potential links with climate mechanisms. However, to determine the mechanism and impact of these interactions at different timescales, further research is awaited.

Supplementary Information The online version contains supplementary material available at https://doi.org/10.1007/s10584-024-03688-4.

Acknowledgements This study was supported by the NSFC (U1803341), the National Key R&D Program of China (2018YFA0606401), and the Higher Education Commission (Ref No. 20-17521/NRPU/R&D/HEC/2021).

Author contribution Adam Khan conducted the field survey, data collection and wrote first draft of the manuscript. Feng Chen revised the first draft of this manuscript. Heli Zhang improved modeling of this manuscript. He performed the correlation and comparison analysis. Sidra Saleem improved the manuscript to move scientific depth as per scientific novelty. Hamada E. Ali improved the quality of the manuscript and provided English language. Weipeng Yue and Martín Hadad done analysis of SASMI, AMO, ENSO, solar activities, and extract map for this manuscript via ARCGIS.

Funding This study was supported by the NSFC (U1803341), the National Key R&D Program of China (2018YFA0606401), and Higher Education Commission (Ref No. 20–17521/NRPU/R&D/HEC/2021).

Data availability Data of this manuscript can be available on request.

Declarations

Consent for publication The authors have provided consent for the publication of this manuscript.

Competing interests The authors declare no competing interests.

References

Ahmad S, Zhu L, Yasmeen S, Zhang Y, Li Z, Ullah S, Han S, Wang X (2020) A 424-year tree-ring-based Palmer Drought Severity Index reconstruction of Cedrus deodara D. Don from the Hindu Kush range of Pakistan: linkages to ocean oscillations. Clim past 16:783–798

Ahmed M (1989) Tree-ring chronologies of Abies pindrow (Royle) spach from Himalyan region of Pakistan. Pak J Bot 21:347–354

Ahmed M, Palmer J, Khan N, Wahab M, Fenwick P, Esper J, Cook E (2011) The dendroclimatic potential of conifers from northern Pakistan. Dendrochronologia 29:77–88

Allan R, Lindesay J, Parker D (1996) El Niño southern oscillation & climatic variability. CSIRO publishing

Asad F, Zhu H, Zhang H, Liang E, Muhammad S, Farhan SB, Hussain I, Wazir MA, Ahmed M, Esper J (2016) Are Karakoram temperatures out of phase compared to hemispheric trends? Clim Dyn 48:3381–3390

Betzler C, Eberli GP, Kroon D, Wright JD, Swart PK, Nath BN, Alvarez-Zarikian CA, Alonso-García M, Bialik OM, Blättler CL (2016) The abrupt onset of the modern South Asian Monsoon winds. Sci Rep 6:1–10

Bhandari S, Speer JH, Khan A, Ahmed M (2020) Drought signal in the tree rings of three conifer species from Northern Pakistan. Dendrochronologia 63:125742

Biondi F, Waikul K (2004) DENDROCLIM2002: A C++ program for statistical calibration of climate signals in tree-ring chronologies. Comput Geosci 30:303–311

Borgaonkar HP, Sikder A, Ram S, Pant GB (2010) El Niño and related monsoon drought signals in 523-year-long ring width records of teak (Tectona grandis LF) trees from south India. Palaeogeogr Palaeoclimatol Palaeoecol 285:74–84

Burgers G, Jin FF, Van Oldenborgh GJ (2005) The simplest ENSO recharge oscillator. Geophys Res Lett 32:L13706. https://doi.org/10.1029/2005GL022951

Cai Q, Liu Y, Liu H, Ren J (2015) Reconstruction of drought variability in North China and its association with sea surface temperature in the joining area of Asia and Indian-Pacific Ocean. Palaeogeogr Palaeoclimatol Palaeoecol 417:554–560

Chen F, Shang H, Yuan Y (2016) Dry/wet variations in the eastern Tien Shan (China) since AD 1725 based on Schrenk spruce (Picea schrenkiana Fisch. et Mey) tree rings. Dendrochronologia 40:110–116
Chen F, Zhang T, Seim A, Yu S, Zhang R, Linderholm HW, Kobuliev ZV, Ahmadov A, Kodirov A (2019) Juniper tree-ring data from the Kuramin Range (Northern Tajikistan) reveals changing summer drought signals in western Central Asia. Forests 10:505
Chen F, Opała-Owczarek M, Khan A, Zhang H, Owczarek P, Chen Y, Ahmed M, Chen F (2021) Late twentieth century rapid increase in high Asian seasonal snow and glacier-derived streamflow tracked by tree rings of the upper Indus River basin. Environ Res Lett 16:094055
Cook E, Kairiukstis L (1990) Methods of Dendrochronology: applications in the environmental sciences. Kluwer, Dordrecht, p 394
Cook ER, Anchukaitis KJ, Buckley BM, D'Arrigo RD, Jacoby GC, Wright WE (2010) Asian monsoon failure and megadrought during the last millennium. Science 328:486–489
Cook ER, Palmer JG, Ahmed M, Woodhouse CA, Fenwick P, Zafar MU, Wahab M, Khan N (2013) Five centuries of Upper Indus River flow from tree rings. J Hydrol 486:365–375
Cook ER, Briffa K, Shiyatov S, Mazepa V (1990) Tree-ring standardization and growth-trend estimation. Methods of dendrochronology: applications in the environmental sciences. Springer Science & Business Media, Berlin, pp 104–123
de Oliveira-Júnior JF, de Gois G, de BodasTerassi PM, da Silva Junior CA, Blanco CJC, Sobral BS, Gasparini KAC (2018) Drought severity based on the SPI index and its relation to the ENSO and PDO climatic variability modes in the regions North and Northwest of the State of Rio de Janeiro-Brazil. Atmos Res 212:91–105
Durbin J, Watson GS (1950) Testing for serial correlation in least squares regression: I. Biometrika 37:409–428
Easterling DR, Evans J, Groisman PY, Karl TR, Kunkel KE, Ambenje P (2000) Observed variability and trends in extreme climate events: a brief review. Bull Am Meteor Soc 81:417–426
Esper J, Shiyatov S, Mazepa V, Wilson R, Graybill D, Funkhouser G (2003) Temperature-sensitive Tien Shan tree ring chronologies show multi-centennial growth trends. Clim Dyn 21:699–706
Fang K, Gou X, Chen F, D'Arrigo R, Li J (2010) Tree-ring based drought reconstruction for the Guiqing Mountain (China): linkages to the Indian and Pacific Oceans. Int J Climatol 30:1137–1145
Fang K, Gou X, Chen F, Liu C, Davi N, Li J, Zhao Z, Li Y (2012) Tree-ring based reconstruction of drought variability (1615–2009) in the Kongtong Mountain area, northern China. Global Planet Change 80:190–197
Fritts H (1976) Tree rings and climate. Elsevier
Gaire NP, Dhakal YR, Shah SK, Fan Z-X, Bräuning A, Thapa UK, Bhandari S, Aryal S, Bhuju DR (2019) Drought (scPDSI) reconstruction of trans-Himalayan region of central Himalaya using Pinus wallichiana tree-rings. Palaeogeogr Palaeoclimatol Palaeoecol 514:251–264
Gutiérrez E, Campelo F, Camarero JJ, Ribas M, Muntán E, Nabais C, Freitas H (2011) Climate controls act at different scales on the seasonal pattern of Quercus ilex L. stem radial increments in NE Spain. Trees 25:637–646
Holmes RL (1983) Computer-assisted quality control in tree-ring dating and measurement. Tree-ring Bulletin 43:69–78
Hong-yan L, Li-jun X, Xiao-jun W (2015) Relationship between solar activity and flood/drought disasters of the Second Songhua river basin. J Water Clim Change 6:578–585
Huang J, Yu H, Guan X, Wang G, Guo R (2016) Accelerated dryland expansion under climate change. Nat Clim Chang 6:166–171
IPCC (2007) Climate change 2007-synthesis report. Contribution of Working groups I II and III to the fourth assessment report of the Anpassungsstrategien und Klimaschutzaktivitäten
Khan N, Ahmed M, Shaukat SS (2013) Climatic signal in tree-ring chronologies of Cedrus deodara from Chitral Hindukush Range of Pakistan. Geochronometria 40:195–207
Khan A, Chen F, Ahmed M, Zafar MU (2019) Rainfall reconstruction for the Karakoram region in Pakistan since 1540 CE reveals out-of-phase relationship in rainfall between the southern and northern slopes of the Hindukush-Karakorum-Western Himalaya region. Int J Climatol 40:52–62
Khan A, Ahmed M, Gaire NP, Iqbal J, Siddiqui MF, Khan A, Shah M, Hazrat A, Saqib NU, Mashwani WK (2021) Tree-ring-based temperature reconstruction from the western Himalayan region in northern Pakistan since 1705 CE. Arab J Geosci 14:1–12
Krishna K, Rao SR (2010) ENSO-related modulation of coastal upwelling along the central east coast of India (vol 10, pg 19, 2009). Atmospheric Science Letters 11(3):239–239
Kumar KK, Rajagopalan B, Hoerling M, Bates G, Cane M (2006) Unraveling the mystery of Indian monsoon failure during El Niño. Science 314:115–119
Kumar P, Kumar RK, Rajeevan M, Sahai AK (2007) On the recent strengthening of the relationship between ENSO and northeast monsoon rainfall over South Asia. Clim Dyn 28:649–660

Li J, Zeng Q (2002) A unified monsoon index. Geophys Res Lett 29(8):115–121
Liang E, Liu X, Yuan Y, Qin N, Fang X, Huang L, Zhu H, Wang L, Shao X (2006) The 1920s drought recorded by tree rings and historical documents in the semi-arid and arid areas of northern China. Clim Change 79:403–432
Liu Y, Bao G, Song H, Cai Q, Sun J (2009) Precipitation reconstruction from Hailar pine (Pinus sylvestris var. mongolica) tree rings in the Hailar region, Inner Mongolia, China back to 1865 AD. Palaeogeogr Palaeoclimatol Palaeoecol 282:81–87
Malik A, Brönnimann S, Stickler A, Raible CC, Muthers S, Anet J, Rozanov E, Schmutz W (2017) Decadal to multi-decadal scale variability of Indian summer monsoon rainfall in the coupled ocean-atmosphere-chemistry climate model SOCOL-MPIOM. Clim Dyn 49:3551–3572
Mann ME, Lees JM (1996) Robust estimation of background noise and signal detection in climatic time series. Clim Change 33:409–445
Mayer C, Lambrecht A, Mihalcea C, Belo M, Diolaiuti G, Smiraglia C, Bashir F (2010) Analysis of glacial meltwater in Bagrot Valley, Karakoram. Mt Res Dev 30:169–177
Muscheler R, Joos F, Beer J, Müller SA, Vonmoos M, Snowball I (2007) Solar activity during the last 1000 yr inferred from radionuclide records. Quatern Sci Rev 26:82–97
Palmer JG, Cook ER, Turney CS, Allen K, Fenwick P, Cook BI, O'Donnell A, Lough J, Grierson P, Baker P (2015) Drought variability in the eastern Australia and New Zealand summer drought atlas (ANZDA, CE 1500–2012) modulated by the Interdecadal Pacific Oscillation. Environ Res Lett 10:124002
Pederson N, Jacoby GC, D'Arrigo RD, Cook ER, Buckley BM, Dugarjav C, Mijiddorj R (2001) Hydrometeorological reconstructions for northeastern Mongolia derived from tree rings: 1651–1995. J Clim 14:872–881
Pederson N, Hessl AE, Baatarbileg N, Anchukaitis KJ, Di Cosmo N (2014) Pluvials, droughts, the Mongol Empire, and modern Mongolia. Proc Natl Acad Sci 111:4375–4379
Peng J-f, Liu Y-z (2013) Reconstructed droughts for the northeastern Tibetan Plateau since AD 1411 and its linkages to the Pacific, Indian and Atlantic Oceans. Quatern Int 283:98–106
Ram S (2012) Tree growth–climate relationships of conifer trees and reconstruction of summer season Palmer Drought Severity Index (PDSI) at Pahalgam in Srinagar, India. Quatern Int 254:152–158
Rao MP, Cook ER, Cook BI, Palmer JG, Uriarte M, Devineni N, Lall U, D'Arrigo RD, Woodhouse CA, Ahmed M (2018) Six centuries of Upper Indus Basin streamflow variability and its climatic drivers. Water Resour Res 54:5687–5701
Sano M, Buckley BM, Sweda T (2009) Tree-ring based hydroclimate reconstruction over northern Vietnam from Fokienia hodginsii: eighteenth century mega-drought and tropical Pacific influence. Clim Dyn 33:331–340. https://doi.org/10.1007/s00382-008-0454-y
Sano M, Ramesh R, Sheshshayee M, Sukumar R (2012) Increasing aridity over the past 223 years in the Nepal Himalaya inferred from a tree-ring δ18O chronology. The Holocene 22:809–817
Schoennagel T, Veblen TT, Romme WH, Sibold JS, Cook ER (2005) ENSO and PDO variability affect drought-induced fire occurrence in Rocky Mountain subalpine forests. Ecol Appl 15:2000–2014
Shah SMA, Zeb A, Mahmood S (2010) The rainfall activity and temperatures distribution over NWFP during the pre-monsoon season (April to June) 2009. Pakistan J Meteorol 6:1–20
Shi F, Li J, Wilson RJ (2014) A tree-ring reconstruction of the South Asian summer monsoon index over the past millennium. Sci Rep 4:6739
Shi Z, Xu L, Dong L, Gao J, Yang X, Lü S, Feng C, Shang J, Song A, Guo H (2016) Growth–climate response and drought reconstruction from tree-ring of Mongolian pine in Hulunbuir, Northeast China. Journal of Plant Ecology 9:51–60
Shi H, Wang B, Cook ER, Liu J, Liu F (2018) Asian summer precipitation over the past 544 years reconstructed by merging tree rings and historical documentary records. J Clim 31:7845–7861
Singh V, Yadav RR, Gupta AK, Kotlia BS, Singh J, Yadava AK, Singh AK, Misra KG (2017) Tree ring drought records from Kishtwar, Jammu and Kashmir, northwest Himalaya, India. Quatern Int 444:53–64
Singh V, Misra KG, Singh AD, Yadav RR (2022) Increasing incidence of droughts since later part of Little Ice Age over north-western Himalaya. India. Journal of Geophysical Research: Atmospheres 127:e2021JD036052
Sinha A, Cannariato KG, Stott LD, Cheng H, Edwards RL, Yadava MG, Ramesh R, Singh IB (2007) A 900-year (600 to 1500 AD) record of the Indian summer monsoon precipitation from the core monsoon zone of India. Geophys Res Lett 34:L16707. https://doi.org/10.1029/2007GL030431
Sinha A, Berkelhammer M, Stott L, Mudelsee M, Cheng H, Biswas J (2011) The leading mode of Indian Summer Monsoon precipitation variability during the last millennium. Geophys Res Lett p 38. https://doi.org/10.1029/2011GL047713
Speer JH (2010) Fundamentals of tree-ring research. University of Arizona Press
Treydte KS, Schleser GH, Helle G, Frank DC, Winiger M, Haug GH, Esper J (2006) The twentieth century was the wettest period in northern Pakistan over the past millennium. Nature 440:1179–1182

van der Schrier G, Barichivich J, Briffa K, Jones P (2013) A scPDSI-based global data set of dry and wet spells for 1901–2009. J Geophys Res: Atmospheres 118:4025–4048
van Oldenborgh GJ, te Raa LA, Dijkstra HA, Philip SY (2009) Frequency- or amplitude-dependent effects of the Atlantic meridional overturning on the tropical Pacific Ocean. Ocean Sci 15:293–301. https://doi.org/10.5194/os-5-293-2009
Wang B, Biasutti M, Byrne MP, Castro C, Chang C-P, Cook K, Fu R, Grimm AM, Ha K-J, Hendon H (2021) Monsoons climate change assessment. Bull Am Meteor Soc 102:E1–E19
Webster PJ, Magana VO, Palmer T, Shukla J, Tomas R, Yanai M, Yasunari T (1998) Monsoons: processes, predictability, and the prospects for prediction. J Geophys Res: Oceans 103:14451–14510
Wigley TM, Briffa KR, Jones PD (1984) On the average value of correlated time series, with applications in dendroclimatology and hydrometeorology. J Appl Meteorol Climatol 23:201–213
Winiger M, Gumpert M, Yamout H (2005) Karakorum–Hindukush–western Himalaya: assessing high-altitude water resources. Hydrol Process: Int J 19:2329–2338
Xiang Q, Carter G, Rushforth K (2013) Abies pindrow. The IUCN Red List of Threatened Species
Yadav RR, Gupta AK, Kotlia BS, Singh V, Misra KG, Yadava AK, Singh AK (2017) Recent wetting and glacier expansion in the northwest Himalaya and Karakoram. Sci Rep 7:1–8
Yang B, Qin C, Bräuning A, Burchardt I, Liu J (2011) Rainfall history for the Hexi Corridor in the arid northwest China during the past 620 years derived from tree rings. Int J Climatol 31:1166–1176
Zafar MU, Ahmed M, Farooq MA, Akbar M, Hussain A (2010) Standardized tree ring chronologies of Picea smithiana from two new sites of Northern area Pakistan. World Appl Sci J 11:1531–1536
Zafar MU, Ahmed M, Rao MP, Buckley BM, Khan N, Wahab M, Palmer J (2015) Karakorum temperature out of phase with hemispheric trends for the past five centuries. Clim Dyn 46:1943–1952
Zhang Y, Tian Q, Gou X, Chen F, Leavitt SW, Wang Y (2011) Annual precipitation reconstruction since AD 775 based on tree rings from the Qilian Mountains, northwestern China. Int J Climatol 31:371–381
Zhang R, Shang H, Yu S, He Q, Yuan Y, Bolatov K, Mambetov BT (2017) Tree-ring-based precipitation reconstruction in southern Kazakhstan, reveals drought variability since AD 1770. Int J Climatol 37:741–750

Authors and Affiliations

Adam Khan[1] · Feng Chen[2] · Heli Zhang[2] · Sidra Saleem[3] · Hamada E. Ali[4] · Weipeng Yue[2] · Martín Hadad[5,6]

✉ Adam Khan
adam@ulm.edu.pk

Feng Chen
feng653@163.com

[1] Department of Botany, University of Lakki Marwat, Lakki Marwat, KP, Pakistan

[2] Yunnan Key Laboratory of International Rivers and Transboundary Eco-Security, Institute of International Rivers and Eco-Security, Yunnan University, Kunming, China

[3] Department of Botany, Abdul Wali Khan University Mardan, Mardan, KP, Pakistan

[4] Department of Biology, College of Science, Sultan Qaboos University, Muscat 123, Oman

[5] Laboratorio de Dendrocronología de Zonas Áridas. CIGEOBIO (CONICET-UNSJ), San Juan, Argentina

[6] Gabinete de Geología Ambiental (INGEO-UNSJ), Av. Ignacio de La Roza 590 (Oeste), J5402DCS Rivadavia, San Juan, Argentina